



## X-RAY COMPUTED TOMOGRAPHY OF TWO MAMMOTH CALF MUMMIES

DANIEL C. FISHER,<sup>1</sup> ETHAN A. SHIRLEY,<sup>1</sup> CHRISTOPHER D. WHALEN,<sup>1</sup> ZACHARY T. CALAMARI,<sup>2</sup>  
ADAM N. ROUNTREY,<sup>1</sup> ALEXEI N. TIKHONOV,<sup>3</sup> BERNARD BUIGUES,<sup>4</sup> FRÉDÉRIC LACOMBAT,<sup>5</sup>  
SEMYON GRIGORIEV,<sup>6</sup> AND PIOTR A. LAZAREV<sup>6†</sup>

<sup>1</sup>Museum of Paleontology, University of Michigan, 1109 Geddes Ave., Ann Arbor, MI 48109-1079, USA, <dcfisher@umich.edu>; <arountre@umich.edu>; <sup>2</sup>Richard Gilder Graduate School, American Museum of Natural History, Central Park West at 79th Street, New York, NY 10024, USA, <zcalamari@amnh.org>; <sup>3</sup>Zoological Institute, Russian Academy of Sciences, Universitetskaya nab.1, Saint-Petersburg, 199034, Russia, <atikh@mail.ru>; <sup>4</sup>International Mammoth Committee, Place Louis XIV, St. Jean de Luz, 64500, France, <b.buigues@mammuthus.org>; <sup>5</sup>Musée de Paléontologie de Chilhac, place de l'Église, Chilhac, 43380, France, <flacombat@gmail.com>; and <sup>6</sup>Museum of Mammoth, Institute of Applied Ecology of the North, North-Eastern Federal University, 48 Kulakovskogo St., Yakutsk, 677000, Republic of Sakha (Yakutia), Russia, <g\_semen@mail.ru> † deceased

**ABSTRACT**—Two female woolly mammoth neonates from permafrost in the Siberian Arctic are the most complete mammoth specimens known. Lyuba, found on the Yamal Peninsula, and Khroma, from northernmost Yakutia, died at ages of approximately one and two months, respectively. Both specimens were CT-scanned, yielding detailed information on the stage of development of their dentition and skeleton and insight into conditions associated with death. Both mammoths died after aspirating mud. Khroma's body was frozen soon after death, leaving her tissues in excellent condition, whereas Lyuba's body underwent postmortem changes that resulted in authigenic formation of nodules of the mineral vivianite associated with her cranium and within diaphyses of long bones. CT data provide the only comprehensive approach to mapping vivianite distribution. Three-dimensional modeling and measurement of segmented long bones permits comparison between these individuals and with previously recovered specimens. CT scans of long bones and foot bones show developmental features such as density gradients that reveal ossification centers. The braincase of Khroma was segmented to show the approximate morphology of the brain; its volume is slightly less (~2,300 cm<sup>3</sup>) than that of neonate elephants (~2,500 cm<sup>3</sup>). Lyuba's premaxillae are more gracile than those of Khroma, possibly a result of temporal and/or geographic variation but probably also reflective of their age difference. Segmentation of CT data and 3-D modeling software were used to produce models of teeth that were too complex for traditional molding and casting techniques.

### INTRODUCTION

WOOLLY MAMMOTHS (*Mammuthus primigenius* [Blumenbach 1799]) were the latest-surviving representatives of a predominantly Eurasian lineage of mammoths that occupied vast areas of northern steppe and sub-glacial habitat across Eurasia. They are interpreted as most closely related to populations of *M. trogontherii* (Pohlig, 1885) in northeast Asia ca. 700 Ka, and by 200 Ka, their range had expanded into Europe (Lister and Sher, 2001; Lister et al., 2005). They also dispersed eastward into North America, with a complex subsequent history of population movements and gene flow resolvable only through studies of ancient DNA (e.g., Barnes et al., 2007; Debruyne et al., 2008). In the late Pleistocene, woolly mammoths occupied parts of North America south of the continental ice sheets, where they encountered and apparently hybridized (Enk et al., 2011) with *M. columbi* (Falconer, 1857), derived from an earlier range extension into North America by *M. trogontherii* (Lister and Bahn, 2007) or perhaps by its close relative, *M. meridionalis* (Nesti, 1825). The last woolly mammoths lived on Wrangel Island (off the northeast coast of Siberia) until 3,700 yrBP (Vartanyan et al., 1993, 2008).

Much of the history of *M. primigenius* is represented by abundant, but usually isolated, dental and skeletal elements, and these are the typical focus for taxonomic, radiocarbon, and ancient DNA studies. However, the species is also notable for the occurrence of rare, articulated specimens, some with preserved soft tissue (e.g., Tolmachoff, 1929). Despite this apparent wealth of information, most of the classic specimens were found before technologies such as computed tomography were available, and the condition of many of them degraded

before they could be studied as thoroughly as would be possible today. Moreover, it is only with the emergence of studies of mammoth life history (e.g., Fisher, 1996, 2009; Rountrey et al., 2007; Rountrey, 2009; Metcalfe et al., 2010) that the importance of documenting rates and patterns of skeletal and dental development has become clear. A rapidly developing literature (e.g., Maschenko, 2002; Maschenko et al., 2005; Boeskorov et al., 2007) has taken up the challenge of integrating developmental data on multiple, isolated finds, but one of the principal difficulties is always to calibrate comparisons according to the age of each individual. This has typically been done by comparing the stage of development of associated dental material to patterns of timing in the dental development of extant elephants, but this approach necessarily treats as constant some of the features whose evolutionary history we would most like to explore. In contrast, our work bases age assessment on features of dental histology, freeing our results from assumptions about the evolutionary stability of details of timing of dental development. In addition, by focusing on relatively complete specimens, we leverage our age determinations to apply to the entire body. By combining this approach with use of x-ray computed tomography (CT), we have the opportunity for new morphological and developmental insights and sometimes incidental taphonomic insights as well.

Two recent discoveries of nearly complete, frozen bodies of woolly mammoth calves, Lyuba (Kosintsev et al., 2010) and Khroma (Lazarev et al., 2010), from permafrost settings in the Siberian Arctic provide a unique opportunity to enhance our understanding of early stages of development. Because of the remarkable preservation of these specimens, stringent conditions were placed on their study. Some dissection and limited

sampling were allowed (e.g., for detailed study of intestinal contents and elements of the dentition; Fisher et al., 2012; Rountrey et al., 2012; Kosintsev et al., 2012; van Geel et al., 2011), but both specimens were to be left mostly intact. CT scans offered a non-destructive means of visualizing and analyzing much of their anatomy without compromising exhibit potential or options for future analysis. Our goal here is to contribute to the osteology of woolly mammoths and illustrate the potential of CT methods.

#### MATERIAL

Lyuba was found on the bank of the Yuribei River, on the Yamal Peninsula, in May 2007 (Kosintsev et al., 2010) and subsequently accessioned by the Shemanovskiy Museum and Exhibition Center (in Salekhard, Yamalo-Nenets Autonomous Okrug, Russian Federation). When recovered, she was frozen and partially dehydrated, having lost about half her expected moisture content. Otherwise, she appeared to be intact, except for loss of most of her hair and all of her nails. Following transport to the nearest village, she was left unsecured, and domestic dogs gnawed off most of her tail and a portion of her right ear. The external appearance of her urogenital tract suggested she was female, and subsequent analysis of her DNA confirmed this (R. Debruyne, personal commun., 2010). During necropsy, we realized that her tissues were acidic and that structures composed predominantly of Type 1 collagen (e.g., periodontal ligament, oral mucosa, and fibers connecting muscles to bones) were highly degraded (Fisher et al., 2012, fig. 4). In her facial region, while removing teeth for study, we encountered botryoidal masses (most with diameters ranging from 2 to 8 mm) composed of radiating, acicular crystals of the hydrated iron phosphate mineral vivianite,  $\text{Fe}_3(\text{PO}_4)_2 \cdot 8(\text{H}_2\text{O})$ . These and other observations led to the proposal that Lyuba's body had been colonized postmortem by lactic-acid-producing bacteria and that acid fixation had enhanced the resistance of her tissues to bacterially mediated decay and scavenging during an exposure history of nearly one year following exhumation and transport in the ice-out flood event of the previous spring (Fisher et al., 2012).

Histologic analysis of Lyuba's left upper and lower second deciduous premolars identified in each a neonatal line marking the time of her birth, and counts of daily dentin increments showed that she died only 30–35 days later (Rountrey et al., 2012). Stable isotope profiles and dentin increments allowed us to identify her season of birth as spring (but before the onset of new plant growth) and suggested a gestation period of ca. 20 months, comparable to that of extant elephants (Rountrey et al., 2012). At death, she was well nourished and healthy, judging from the abundance of subcutaneous fat and milk residues in her intestine; we therefore interpret her developmental trajectory as normal for her species. Our AMS assay of her age places her at ca. 41,800  $^{14}\text{C}$  yrBP (Fisher et al., 2012).

Khroma was found in October 2008, near the Khroma River in northern Yakutia (Lazarev et al., 2010), frozen in permafrost in an upright position. After recovery in May 2009, she was brought to the Mammoth Museum, Institute of Applied Ecology of the North, North-East Federal University (in Yakutsk, Sakha Republic [Yakutia], Russian Federation). Her head, trunk, and shoulders had been exposed by seasonal melting and subsequent erosion of adjacent sediment, but these parts of her body were initially intact, while the rest of her body, lodged more deeply within the permafrost, remained frozen. However, by the time a party arrived to collect the specimen, ravens, and possibly arctic foxes, had scavenged exposed portions. She thus lost the distal and middle parts of her trunk, most soft tissues from the dorsal

aspect of her skull, the entire fat hump that we suspect (following analogy to Lyuba; Fisher et al., 2012) covered the dorsal aspect of her neck, and the contents (heart and lungs) of her pleural cavity, bounded posteriorly by the intact diaphragm. Otherwise, her body was recovered in good condition.

Khroma's sex was initially a matter of debate, but preliminary analysis of her DNA (R. Debruyne, personal commun., 2011) and CT analysis of her urogenital tract (to be discussed elsewhere) confirm her as female. Histologic analysis of Khroma's dentition, revealing her age, is discussed below. Khroma's necropsy revealed abundant subcutaneous fat, a stomach full of undigested milk, and digested milk within her intestines. Her AMS assay returned an “infinite” result, indicating only that her age is greater than 45,000 yrBP.

#### METHODS

A CT scan of Lyuba's fully frozen body was performed prior to any dissection. Open spaces within Lyuba's thorax and abdomen were then examined endoscopically through ports drilled into her left side, after which she underwent two necropsy sessions, for each of which her body was thawed. During the first, we removed the left side of her dentition for detailed study and sampled portions of her small and large intestine through an opening in her left flank. In the second necropsy, we made a larger opening on her left side, allowing examination of her pleural and abdominal cavities. The Shemanovskiy Museum then determined that her body would be treated chemically to resist decay and allowed to desiccate.

At this point we learned we would not be given access to the original CT data. A first attempt to replicate this study was made shortly after Lyuba's chemical treatment, when her moisture content still approximated the semi-desiccated state in which she had been discovered. Staff of the GE Healthcare Institute in Waukesha, Wisconsin used a GE Medical Systems LightSpeed RT16 with a gantry opening 80 cm in diameter, providing an image diameter of 60 cm. Lyuba's dorsoventral height at the time was 85 cm, so we were limited to an anterior scan capturing her head, neck, and part of her right forelimb, and a posterior scan capturing part of her pelvic region and left hind limb. Scan settings were: 120 kVp, 600 mA, and exposure time 800 ms. Uniform cubic voxels were 0.625 mm on a side. The first complete, full-body scan of Lyuba (or of any mammoth, to our knowledge) was conducted by staff of the Nondestructive Evaluation Laboratory of Ford Motor Company in Livonia, Michigan. An Aracor ICT 1500 industrial scanner was used, providing an image diameter of 1 m. For this scan, Lyuba was supported inside a wooden box with her anteroposterior axis vertical. Scan settings were: 9 MVp, 81.6 mA, and exposure time 4.3  $\mu\text{s}$ . Because of time constraints imposed by prior contracts covering her transport from one museum to another, we had only a 17-hr window of time for completion of this scan. Industrial scanners operate more slowly than medical scanners, so this time constraint required a relatively low anteroposterior resolution ( $1 \times 1 \times 3$  mm, rather than the smaller, uniform voxels from medical scans). A second, shorter pass was made over Lyuba's thoracic cavity, offset 1 mm from the first scan, to increase resolution in this important region.

Two sets of CT scans of Khroma were conducted using medical scanners with gantry openings 70 cm in diameter and image diameters of 50 cm. These were done by GE Healthcare at the Centre Hospitalier Universitaire de Clermont-Ferrand, in Clermont-Ferrand, France and by staff at the Centre Hospitalier Emile Roux in Le Puy-en-Velay, France. Both scans were to have been done after Khroma's body had thawed, but this took more time than expected. Data from the Le Puy scan were

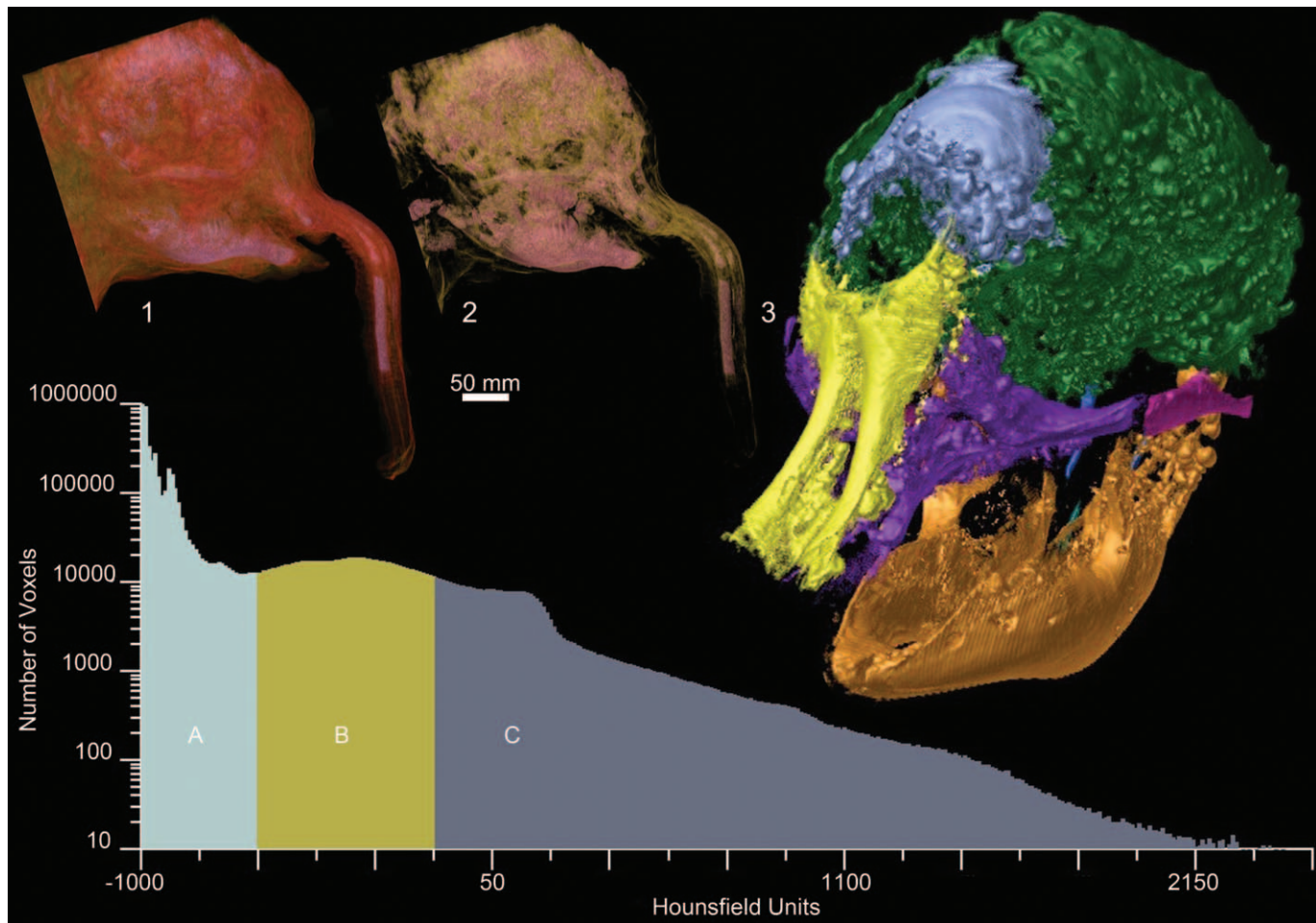


FIGURE 1—Histogram of attenuation values in Hounsfield Units for the GE medical CT scan of Lyuba, with three attenuation ranges (A, B, and C) designated and examples of thresholding and segmentation: 1, part of Lyuba's head after removal of voxels in Hounsfield range A, corresponding to air and Styrofoam packing materials (-1,000 to -660 units); 2, same view of Lyuba after removing also voxels in Hounsfield range B, corresponding to soft tissues including muscle, fat, and dermis (-660 to -125 units); histogram range C shows hard structures, such as bone and mineral deposits (-125 to +2,500 units); Hounsfield values do not correspond to literature values for bone, muscle and fat, due to the partly desiccated nature of the specimen; 3, oblique view of Lyuba's cranium and mandible, with segmentation of some bones. Abbreviations: f, pa=frontal/parietal complex without visible sutures; ju=jugal; ma=mandible; mx=maxillae; na=nasals; pm=premaxillae.

ultimately more useful because this scan occurred when thawing was more complete. Although Khroma's body fit through both gantry openings, data volumes did not include some of the more peripheral portions of the posterior end of the body. At the time of scanning, Khroma had been stored in a freezer for over a year and had no doubt lost considerable moisture. However, her body had not desiccated as thoroughly as Lyuba's, so her scans showed a more nearly normal range of tissue attenuation values. Scan settings in Le Puy, on a GE Medical Systems LightSpeed VCT were: 140 kVp, 590 mA, and 700 ms. Uniform cubic voxels were 1 mm on a side.

Micro CT scans of extracted teeth of both Lyuba and Khroma were conducted at the University of Michigan Dental School in Ann Arbor, Michigan, using a Scanco Medical µCT100. Scan settings were: 90 kVp, 44 µA, and exposure time 500 ms. Uniform cubic voxels were 50 µm on a side.

Data from all medical scans were saved in DICOM format and analyzed using Amira 5.4.0. Lyuba's full-body scan was loaded as raw images, interpolating the first pass over the whole body with the second pass over the thoracic region and normalizing reported R-ranges (controlling exposures). Data were then resampled to transform non-uniform (1×1×2 mm,

1×1×1 mm, and 1×1×3 mm) voxels to a uniform 1×1×1-mm size. Mitchell interpolation between slices was used because comparisons showed that it preserved contrast better than other algorithms.

Data volumes were cropped to minimize memory requirements and remove extraneous features (e.g., the box in which Lyuba was placed for the Ford scan). Skeletal elements and some discernible soft-tissue structures were then segmented (digitally isolated). Segmentation was conducted in stages: first, through thresholding with radiodensity (attenuation) values, then by selecting regions of contiguous voxels falling in a set range of radiodensities, followed by a manual clean-up process at the pixel level in slices along each axis.

Radiodensity is a measure of how much radiation passes through a standard volume of a material. Although it sometimes has values that correlate with physical density, this need not be the case. For example, ice has a radiodensity similar to that of mineralized bone, much higher than that of water. Higher luminance on grayscale displays of CT data (assuming a normal look-up table) indicates higher radiodensity. Hounsfield units, standard for measuring radiodensity in medical scanners, represent air at -1,000 units, water at 0 units, and fat, muscle,

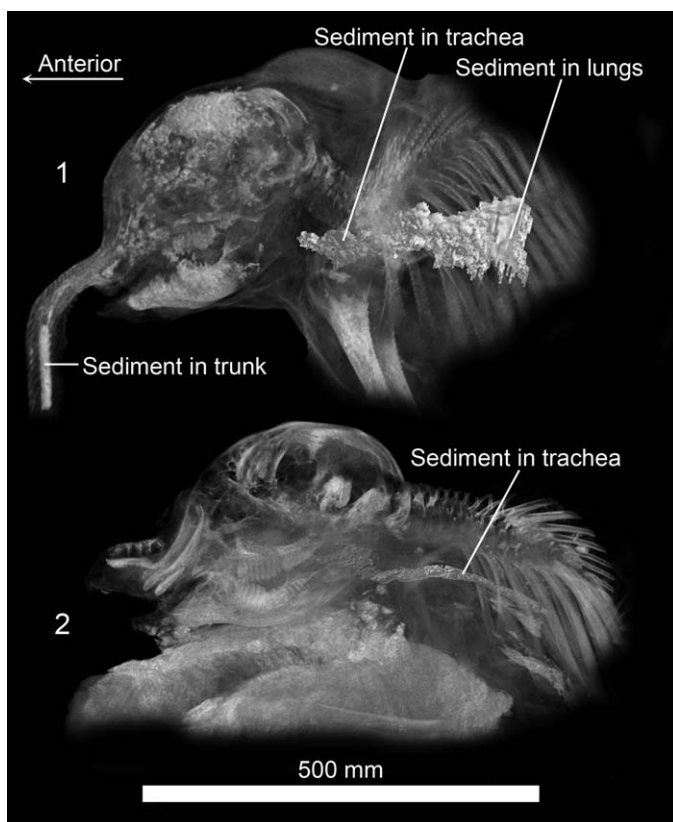


FIGURE 2—Aspirated sediment in both mammoth calves: 1, sediment with a radiodensity in the range of bone can be traced from the pharyngeal region, through the trachea, and into the lung bronchi (from the Ford scan of Lyuba); 2, sediment with a radiodensity in the range of bone (450–900 Hounsfield units) is present in Khroma's oral region, pharyngeal region, and trachea (her lungs were scavenged prior to recovery).

and bone at around –50, 50, and over 400 units, respectively (Hounsfield, 1980). Our medical scans of Lyuba and Khroma reported accurate Hounsfield values, but the Ford scan of Lyuba was scaled differently, requiring us to compute a transformation. More problematic was that Lyuba's desiccation shifted soft-tissue values into the range of –650 to –125 units and made them difficult to differentiate. Bone values were also shifted but generally remained above –125 units (Fig. 1). The radiodensity scale was used in segmentation to help distinguish between materials, but the different levels of hydration in Lyuba and Khroma complicated comparisons.

Images were created using the snapshot function in Amira, and animations were created using custom scripting in the Amira DemoMaker module, displaying volume renderings in which individual segmented parts were highlighted with color-mapping tools. Linear dimensions of segmented volumes were measured in three dimensions in Amira. Volumes were calculated by summing the number of segmented voxels in a given structure. Surfaces were generated and corresponding meshes simplified to fewer faces to reduce computation requirements. They were then exported as \*.stl files and imported into 3-D graphics software (Magics and 3DSOM) for smoothing and other operations (e.g., manual thickening of tooth roots to allow 3-D printing).

#### RESULTS

**Aspirated sediment.**—As described in Fisher et al. (2012), the solid mass of radiodense material (Figs. 1.2, 2.1), occupying the

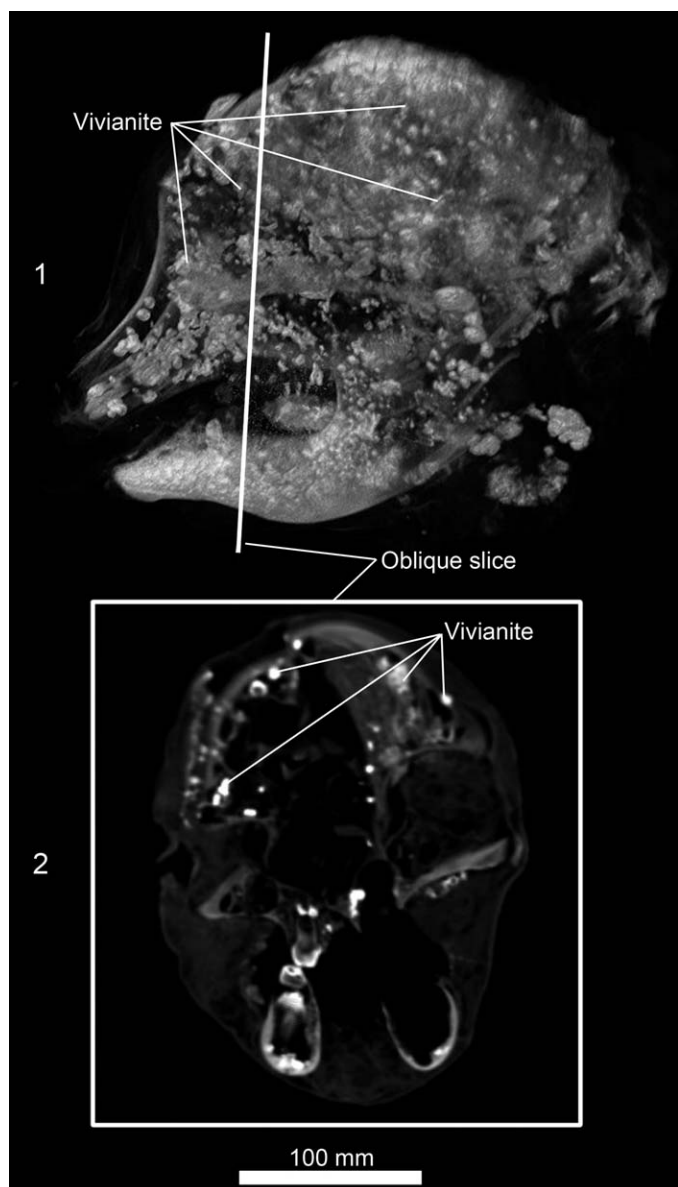


FIGURE 3—Botryoidal vivianite nodules in the cranium of Lyuba as seen in the GE medical scan: 1, left lateral projection with nodules on the surfaces of skull bones, but largely absent from the external surface of the mandible, premaxillae, and maxillae (conical, radiodense structure on the “forehead”, just to the right of the “Vivianite” label is discussed in text); 2, roughly transverse oblique slice through the cranium shown by the line in 1; vivianite nodules have formed within the endocranial space and within diploë of the frontal sinus. Scale applies to both images.

upper middle section of one narial passage in Lyuba's trunk, was present in the original CT scan, done while she was frozen. At that time, the other narial passage was likewise blocked, but no similar material occupied more proximal portions of the trunk. The more diffuse traces of radiodense material seen more proximally (Figs. 1.2, 2.1) appeared only following Lyuba's chemical treatment to resist decay, and we interpret this as sediment that had formerly blocked the narial passages in the middle of the trunk but that was later transported proximally by movement of preservative fluids.

Lyuba's oral cavity was also filled with sediment at necropsy, but this consisted of poorly sorted sand, silt, and clay-sized material that resembled material from the channel margin on which she had been deposited. This evidently had more to do with

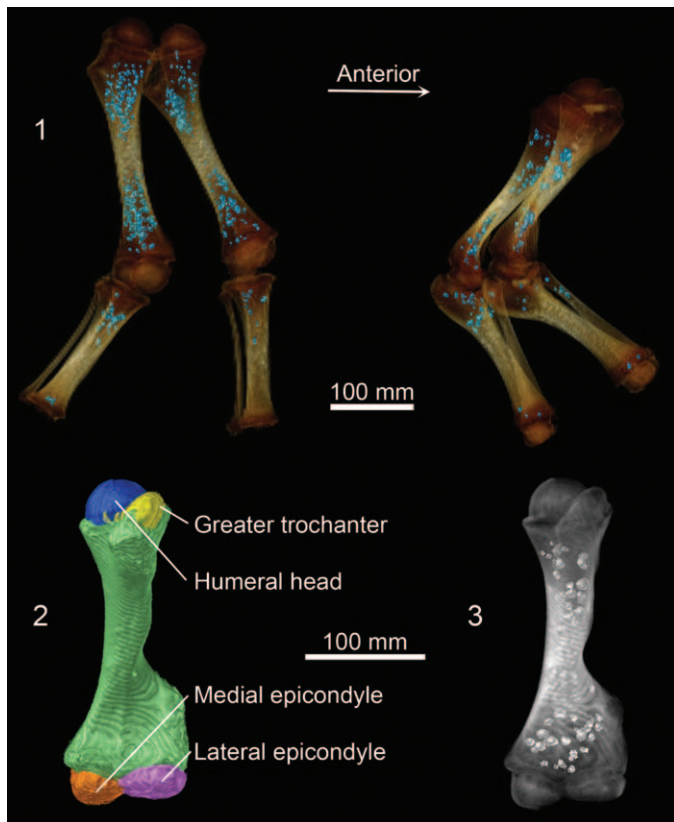


FIGURE 4—Larger elements of Lyuba's appendicular skeleton (without mani and pedes) extracted from the Ford scan: 1, radiodense nodules within developing trabecular spaces in long bones are probably vivianite crystals formed from bone-derived phosphate and blood- and marrow-derived iron; bones show radiodensity disparity between diaphyses and epiphyses; right lateral aspect, hind limbs on left (right ahead of left) and forelimbs on right (right ahead of left); animation in online Supplemental Data file 1 fades and rotates the 3-D rendering in this image (among others) to clarify the location of vivianite and the shapes of bones; 2, left humerus in anterior aspect, diaphysis (green) segmented separately from epiphyseal ossifications (labeled); 3, segmented radiodense nodules show through cortical bone of diaphysis (humerus unsegmented in this image so that nodules show through); common scale for 2 and 3.

her transport and exposure history than with perimortem events (and was mostly removed during the first necropsy).

The second necropsy permitted us to inspect Lyuba's pleural cavity. Her lungs had collapsed, so that they occupied only a small fraction of this space. Some of the larger bronchial passages had ruptured, and out of these openings spilled fine, clay-sized particles of a bright blue material that also coated the walls of the pleural cavity and all tissue surfaces within it. However, cutting into collapsed lung tissue, it was clear that none of this blue powder had dispersed beyond major bronchi into peripheral parts of the lung. The blue powder was identified by x-ray diffraction as vivianite, the same mineral that had been found in nodular form in Lyuba's facial tissues, but here in a completely different habit; clay minerals may also accompany this fine-grained vivianite, but further analysis is required to verify this.

Finally, our CT data show that the material in Lyuba's bronchi, which we know includes vivianite, has the same radiodensity as material filling her trachea, and also the middle parts of the narial passages in her trunk. Fisher et al. (2012) argued that the only mechanism capable of explaining the distribution of this material from Lyuba's trunk to her bronchi was reflexive aspiration of sediment that had become lodged in the proximal portion of her

trunk. With her trachea and bronchi filled, she was unable to breathe and suffocated. Although drowning also deprives a victim of oxygen, flooding the lungs with water would have transported the vivianite present in her respiratory tract into distal alveolar spaces, a pattern for which we see no evidence.

Fine-grained vivianite like that in Lyuba's respiratory tract commonly forms in cold, oxygen-poor lacustrine settings (Manning et al., 1991). Lyuba's tracheal vivianite is most likely from such an environment, providing a clue to the setting in which she died, which would otherwise remain obscure, given the secondary context from which she was recovered.

Although most of Khroma's trunk and lungs were scavenged by the time she was recovered, her CT scan also shows a column of sediment packing her trachea and extending into her oral cavity and narial passages (Fig. 2.2). As with Lyuba, a continuous sediment mass could not have been emplaced along with water, as in drowning, or by currents following death. Only reflexive respiratory movements are likely to transport such a mass, so aspiration of mud and consequent suffocation is again the most likely cause of death. The sediment in Khroma's trachea has a radiodensity in the range of bone but lower than vivianite, so it probably consists of clastics of a more conventional composition. Because both Lyuba and Khroma appear to have been healthy at the time of death, a traumatic demise is not surprising.

*Authigenic vivianite in Lyuba.*—The first vivianite we noticed on Lyuba was localized in small, circular, dermal pits (on the order of one centimeter in diameter) on her left side, where her body had contacted the substrate as she lay beside the Yurubei River for nearly a year. We interpreted the pits as fungal lesions and suspected that in the shade of her underside, near the sediment surface, moisture levels had favored fungal growth. At the time of her recovery, each of these circular features was bright blue, indicative of fine-grained vivianite disseminated within the degraded dermis. With prolonged exposure to oxygen (and after treatment with formalin to kill any fungi), the material in each pit turned to a chalky, reddish brown suggesting a higher oxidation state of iron. Whatever the causes of these changes, this category of vivianite must dominantly reflect the conditions of Lyuba's recent exposure history. The vivianite likely incorporated iron and phosphate ions in Lyuba's tissues or in her immediate environment. Although the grain size is similar to the vivianite in Lyuba's respiratory tract, the host tissue and distributional pattern are completely different.

The second category of vivianite in Lyuba consists of the botryoidal vivianite nodules that we observed in her facial region during necropsy, always in close proximity to bone, but clearly having formed within soft tissue (e.g., muscle, dental pulp, and on the surfaces of unerupted teeth). CT images published here (Figs. 1.3, 2.1, 3) add to the documentation of this category of vivianite and show that nodules comparable to those encountered in necropsy are distributed fairly evenly over the cranium and in spaces such as cranial diploe, which would have been lined originally with mucosa (Fig. 3.2). Their radiodensity is higher than that of surrounding bone. In crystal form and size (up to several millimeters long) this is a profoundly different type of material from the fine-grained vivianite in Lyuba's respiratory tract.

Radiodense material found in long bone diaphyses, especially toward their proximal and distal ends, probably represents a third category of vivianite in Lyuba. Again, images here (Fig. 4) greatly expand on the documentation of this phenomenon offered before (Fisher et al., 2012, fig. 3). Interestingly, this occurrence of radiodense material does not extend to surrounding soft tissue, such as limb musculature. The dense loci at issue here have a smaller average size than the botryoidal nodules associated with Lyuba's facial region, but their attenuation values and form

(small, stellate structures grading into nodular masses) are consistent with interpreting them as nodular, macrocrystalline vivianite comparable to the nodules on Lyuba's cranium. They appear to have grown between bony trabeculae, within spaces that would have been occupied in life by marrow tissue. We were not permitted to cut into long bones and therefore have not sampled this material directly, but the similarity of its CT profile to the nodular vivianite on Lyuba's cranium leads us to interpret it as having the same composition.

In addition to being found on lake bottoms, as noted in our description of aspirated sediment, vivianite is often seen in Pleistocene and Holocene paleontological and archaeological contexts as a fine coating on bone surfaces. In these cases, bones, and often tusks, serve as phosphate sources, while anoxic sediments provide the iron, water, and low-oxygen conditions required for vivianite formation (McGowan and Prangnell, 2006). However, typical vivianite-coated bones and tusks are not associated with preserved soft tissue, and the vivianite covering them differs in crystal size and habit from the soft-tissue-hosted nodules in Lyuba. For "naked" bones and tusks, supplying iron ions to form vivianite is a simple matter of diffusion in sediment pore waters, but the likely source of iron is less clear when vivianite forms inside a body with an intact dermis.

Starting with Lyuba's outer surface, the vivianite within dermal pits has clear analogs on other well-known specimens. The distinctive surface color of the steppe bison mummy "Blue Babe" was traced to dermal "warts" on its head and neck, from which vivianite powder was distributed more broadly (Guthrie, 1990, p. 79). When the vivianite was removed from these features, distinct, hemispherical depressions in the dermis were revealed, exactly matching those on Lyuba. Likewise, the skin of the Tyrolean "Iceman" displayed small "pustules" containing vivianite, on the side that had been oriented downward, against the substrate (Pabst and Hofer, 1998, p. 10). These superficial occurrences thus seem to be a general feature of such mummies.

If Lyuba's tracheal and bronchial vivianite (discussed in the previous section) was aspirated from lake-bottom sediments, and her dermal vivianite (first category discussed in this section) formed in association with recently developed fungal lesions, we still need a mechanism to explain the nodular vivianite (second and third categories discussed in this section). Fisher et al. (2012) proposed a common-cause explanation for nodular vivianite that relates also to their hypotheses for Lyuba's death and postmortem chemical alteration. If Lyuba, immediately before death, was experiencing oxygen deprivation in a cold, wet environment, the mammalian "diving reflex" would have been initiated (Gooden, 1994), with peripheral vasoconstriction shutting down the blood supply to most of the body surface and musculature, with the exception of the facial region, which is necessary for sustaining the reflex (Johansen, 1964). Despite this adaptive response, Lyuba did die, and the volume of blood, and consequently hemoglobin, committed to her brain and facial region (and remaining there after her death) is interpreted as the iron source for the nodular vivianite associated with her cranium. The phosphate source for this and all other nodular vivianite would be phosphate ions made available by postmortem acidification of Lyuba's tissues and dissolution of bone by lactic-acid-producing bacteria. Finally, the diaphyseal occurrences of nodular vivianite can also be explained as a function of iron availability (Fisher et al., 2012). One mechanism behind this may be that long bone diaphyses are loci for blood pooling during peripheral vasoconstriction, but in addition, rapidly growing trabecular bone at the ends of long bone shafts is the prime location for hematopoietic red marrow, with its iron storage and buffering molecules such as ferritin and hemosiderin (Piney, 1922). Both hemoglobin and

hemosiderin dissociate at acid pH (Hanlon et al., 1971; Lillie, 1939) and thus could be sources of free iron within Lyuba's low-pH tissues.

*Age at death.*—The basis for our estimate of Lyuba's age at death was explained in Rountrey et al. (2012), but comparable information has not yet been provided for Khroma. Space constraints preclude detailed treatment here, but we have studied Khroma's right milk tusk, and her right dP<sub>2</sub> and dP<sub>3</sub> with the methods developed for Lyuba's dentition. Khroma's teeth, when removed, were still embedded in the soft tissue in which they occurred in life, including, for her unerupted dP<sub>3</sub>, the enamel organ and associated connective tissue. Upon sectioning her dP<sub>3</sub>, we observed a clearly developed periradicular feature on its root, identical to the external expression of neonatal lines on Lyuba's teeth (Rountrey et al., 2012, fig. 4). In a longitudinal section of this tooth, this feature can be traced into the dentin cross section as the dark band labeled "Neonatal Line" (Fig. 5.1). This feature is a record of the physiological perturbation associated with Khroma's birth. Between this level in the dentin and the pulp surface (which marks the time of death and appears as a "double" line near the upper margin [Fig. 5.1], because it is not exactly perpendicular to the plane of section), we observe faint daily increments in dentin. Counting these requires moving back and forth across the image to continue the count in the best-preserved region for respective time intervals. Our increment marks are too small to be seen clearly (Fig. 5.1), but the enlargement (Fig. 5.2) shows the last 18 days before Khroma's death. We marked 52 daily lines that formed after the neonatal line but suspect we may have missed several poorly preserved features. Allowing for this, we estimate that Khroma's age at death was between 52 and 57 days. The thickness of this entire interval implies a rate of dentin apposition similar to that in Lyuba's dP<sub>3</sub>. This factor and the similarity in position of the neonatal line within the tooth corroborate our age estimate.

*Appendicular skeletons.*—Lyuba and Khroma are mummies with articulated skeletons, but also cartilaginous elements, muscle, fat, connective tissue, organs, and dermis. Because these animals are neonates, their skeletons were still developing at the time of death, providing us with insight into mammoth ontogeny. Unfortunately, developing, unmineralized bone has a radiodensity similar to that of muscle, fat, and connective tissue, making the boundaries of some structures difficult to distinguish. This is exacerbated by desiccation, which tends to shift radiodensity to lower values, but in a non-linear fashion that further compromises discrimination.

Long bones in Lyuba and Khroma were segmented for comparison to each other and to published material. Diaphyses and epiphyses of long bones develop from different ossification centers and are generally distinguishable by recognizing density gradients (Fig. 4.2). Where possible, we segmented diaphyses and epiphyses as independent elements (even though they fuse later in life), because this permits us to focus on what is comparable from specimen to specimen (Fig. 4.3). Although Lyuba and Khroma retain diaphyses and epiphyses in association, most isolated long bones for neonates consist of diaphyses only.

Lyuba's full body scan allows us to examine both forelimbs and hindlimbs. However, because of desiccation (and perhaps bone dissolution), her pedal and manual elements are poorly defined and in many cases not distinguishable from surrounding tissue. In Khroma, the full forelimb is visible, but the sacrum, lateral margins of the pelvis, and parts of the acetabula and femoral heads were outside the CT imaging volume. Thus, we do not compare the femora and pelvis in Khroma with those in Lyuba. Khroma's pedal and manual elements, however, are well defined and were segmented for study.

The scapulae of Lyuba and Khroma were segmented and measured. Their morphologies are similar, but not identical (Fig.

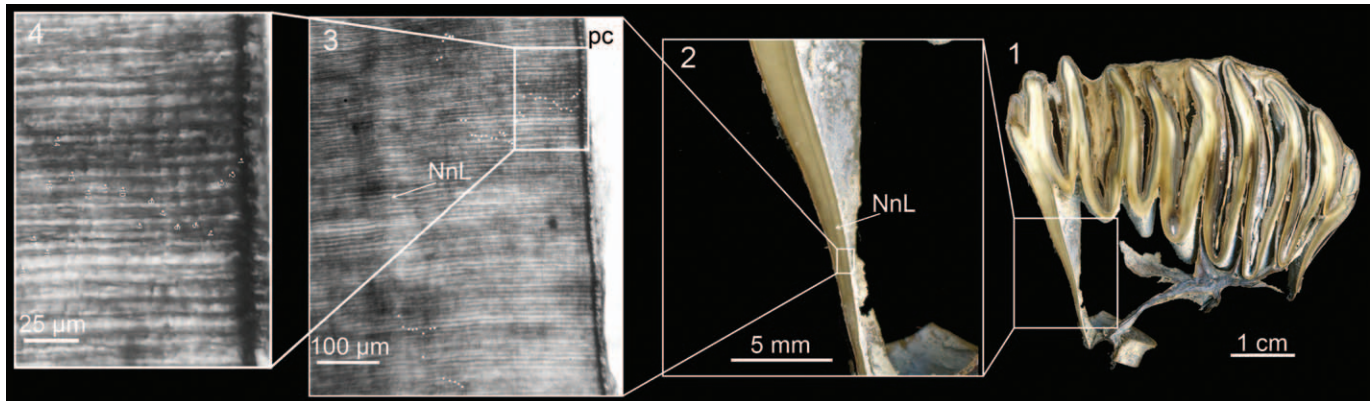


FIGURE 5—Khroma's age, determined from her right dP<sub>3</sub>: 1, right image shows lingual aspect of a slab cut from the right dP<sub>3</sub>, anterior to the left; 2, enlarged view of the anterior root in 1; the dark line running vertically, parallel to the pulp cavity surface, is the neonatal line (NnL); 3, photomicrograph of a thin section of the anterior root, with pulp cavity (pc) surface at right, neonatal line (NnL) at left, and 52 or more daily dentin increments (small white dots) between them; 4, enlargement of area designated in 3, showing increments for last 18 days of life. We estimate Khroma's age at death as 52–57 days.

6). The slender epiphysis along the dorsal and posterior margin of the scapula is included in this segmentation but was partly damaged in Khroma by the scavenging that opened her pleural cavity. The clearest difference between the two individuals is the greater development of the metacromion process in Khroma, where it projects farther posteriorly from the scapular spine (seen from above on the right in Fig. 6). We interpret this as more advanced mineralization in Khroma than in Lyuba, consistent with Khroma's greater age at death (approximately two months, rather than approximately one month for Lyuba). Beyond this, differences are subtle, such as the more sinuous curve of Khroma's scapular blade in dorsal view.

The humeri and ulnae of Lyuba and Khroma (Fig. 7) show subtle differences in shape, such as for the deltopectoral crest on the humerus. These are not clearly related to stage of development but may reflect individual or population-level variation.

The paired ilia, ischia and pubes of Lyuba's pelvis were segmented separately (Fig. 8). The asymmetry seen in the anterior aspect is evidence of compressive forces that have affected much of Lyuba's body, including her cranium. The bone of a mammal this young is likely to respond to stresses in a somewhat plastic manner, and even moderate dissolution, as we infer to have affected Lyuba postmortem, would only increase its susceptibility to distortion. With further work, it might be possible to digitally remove some of this deformation, but we have not attempted this. Parts of the femora that overlap between individuals (given incomplete data on Khroma) are similar, as are tibiae and fibulae.

In the feet, most bones are poorly mineralized (Fig. 9) but show attenuation gradients radiating outward from ossification centers. Many foot bones display distinct nucleation sites, which may coalesce in later stages of development. The calcaneum appears to have two ossification centers, as has been reported in the human osteology literature (Warwick and Williams, 1973, p. 382). One of these is epiphyseal, on the end of the tuber (seen at right in Fig. 9.1), and the other is located nearer the center of mass of the bone. Other tarsal bones have a single ossification center. Metatarsals and phalanges have an epiphyseal and a diaphyseal ossification center (seen in color in Fig. 9.2).

In African elephants, only digits 3 and 4 have distal phalanges that are ossified, whereas in Asian elephants digits 2, 3, and 4 have ossified distal elements (Ramsay and Henry, 2001). It has previously been unclear whether distal phalanges exist, or were ossified, in mammoths, because they are frequently missing from otherwise-complete specimens. These bones would be relatively

small (2–3 cm in diameter), raising the possibility of a preservation bias against them, but sesamoids are similar in size and are commonly preserved. It is possible that distal phalanges exist as cartilaginous elements but never ossify. Proboscideans

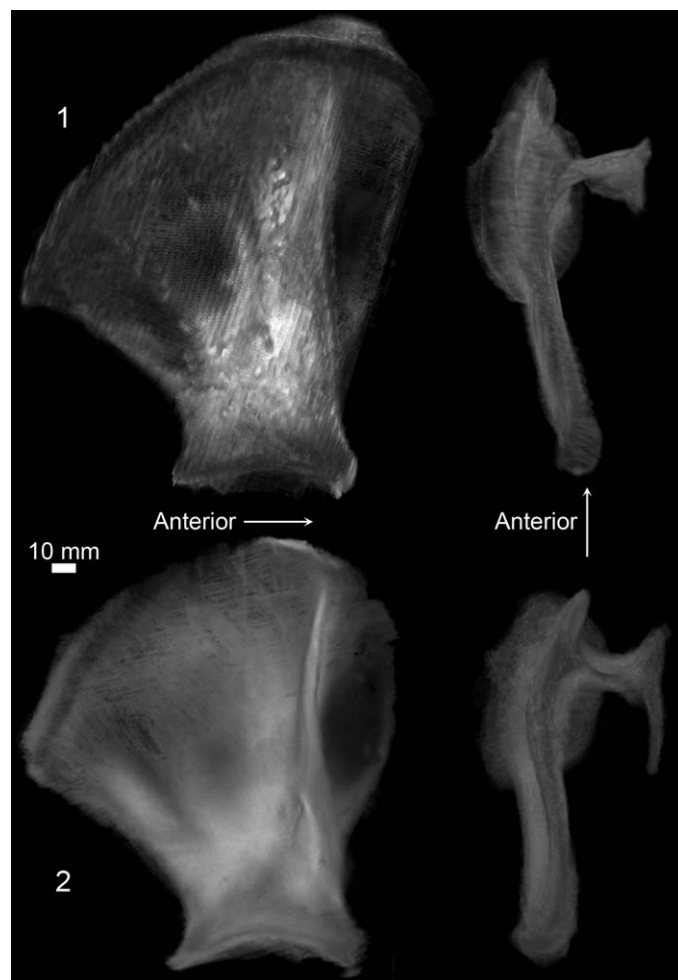


FIGURE 6—Right scapulae of mammoth calves: 1, Lyuba (including dorsal epiphysis), lateral aspect on left, dorsal aspect on right; 2, Khroma (dorsal epiphysis damaged by scavenging), lateral aspect on left, dorsal aspect on right. Scale applies to all figures. The metacromion process is absent (unmineralized) in Lyuba but well developed in Khroma.

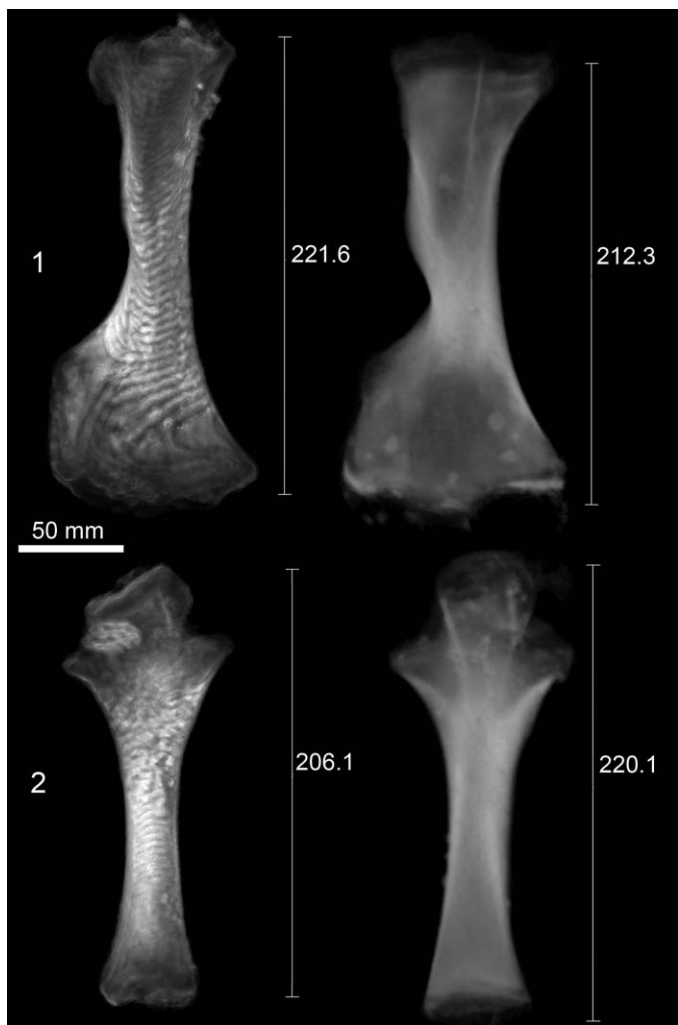


FIGURE 7—Right humeri and ulnae of mammoth calves: 1, humerus of Lyuba on left and Khroma on right, anterior aspect; 2, ulna of Lyuba on left and Khroma on right; anterior aspect. Scale applies to all figures. Maximal diaphyseal measurements at right of each element.

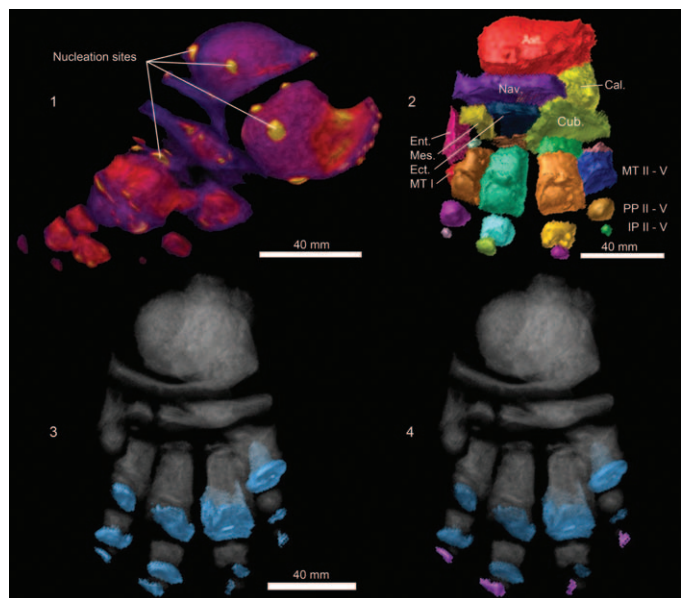


FIGURE 9—Khroma's left hind foot: 1, lateral aspect, anterior to left, showing nucleation sites and epiphyseal ossification center on calcaneum tuber at right; 2, anterior aspect; 3, anterior aspect, synovial joint capsules on digits, light blue; 4, anterior aspect, non-terminal joint capsules light blue and terminal joint capsules purple. Abbreviations: Ast.=astragalus; Cal.=calcaneum; Cub.=cuboid; Ect.=ectocuneiform; Ent.=entocuneiform; IP=intermediate phalanx; Mes.=mesocuneiform; MT=metatarsal; MT I=metatarsal I (red); MT V=metatarsal V (blue diaphysis); PP=proximal phalanx. Separate scales for 1 and 2; common scale for 3 and 4.

walk on a thick fat pad and a thickened dermal layer; distal phalanges distribute weight across the fat pad (Weissengruber, 2006), but it is not clear how their degree of ossification relates to their effectiveness in this role.

We attempted to determine whether Khroma had distal phalanges or not. Unfortunately, we were not able to identify any radiodense element in the position of a distal phalanx. However, we also failed to identify any radiodense element in the position of a metatarsal-phalangeal sesamoid, and we know that these ossify in mammoths. It is thus possible that at the early stage of development seen in Khroma, ossification is not advanced enough to solve this problem by looking for distal phalanges themselves.

We thus decided to take an indirect approach—mapping joint capsules. Interphalangeal joints in mammals are synovial, with fluid-filled connective tissue joint capsules enclosing the locus of bone–bone contact. Even with Khroma's moderate desiccation, synovial fluid has apparently been absorbed by surrounding tissues, leaving an air pocket in its place. These pockets (Fig. 9.3) are easily observed because their radiodensity is like that of air. In this way, we mapped capsules between metatarsals and proximal phalanges, proximal and intermediate phalanges, and also distal to the second through fifth intermediate phalanges. This final capsule indicates that synovial fluid was present prior to desiccation, which implies the existence of some distal phalangeal structure, whether or not it ossified (Fig. 9.4).

*Postcranial axial skeleton.*—We segmented Lyuba's and Khroma's ribs mainly as a foundation for future studies, including analysis of anteroposterior morphologic gradients (Fig. 10.1, 10.2). Ribs are notoriously difficult to attribute to species but may in the future be easier to identify with 3-D morphometric analyses. Lyuba's ribcage was laterally compressed and twisted by postmortem compressional stresses. The left ribs are most severely deformed, but the instances of physical disruption all



FIGURE 8—Lyuba's pelvis: 1, anterior aspect; 2, right lateral aspect. Scale applies to both figures. Much of the dorsolateral expanse of the ilia appears dark because it is relatively thin and not yet well ossified at this stage of ontogeny.

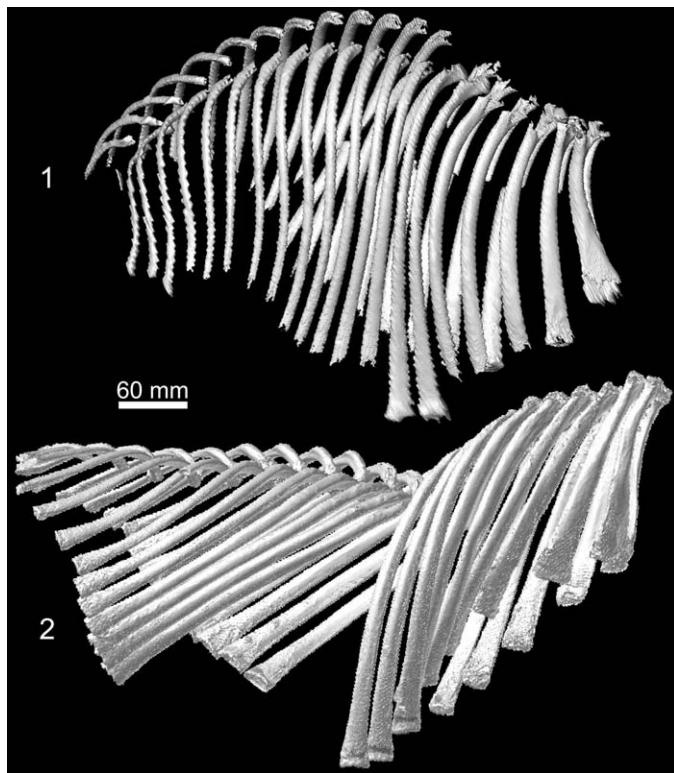


FIGURE 10—Rib series of mammoth calves (orthographic projections): 1, Lyuba's ribcage in right lateral aspect (ribs on the left side were cut during the second necropsy); 2, Khroma's ribcage in right lateral aspect (interruption of rib sequence caused by break in vertebral column). Scale applies to both images.

derive from necropsy. Khroma's ribs are mostly intact, but some were broken proximally during the scavenging that immediately preceded her recovery.

Lyuba's vertebral column is completely intact and in life position. In Khroma, the seventh thoracic vertebra, T7, is separated from T8, and the two halves of the column are displaced at the break. This breakage and displacement must have occurred before Khroma's recent scavenging, because this part of her body was still in the permafrost when she was recovered.

**Khroma's cranial endocast.**—Eutherian neonatal brain size varies with maternal basal metabolic rate and duration of gestation (Sacher, 1974). In Lyuba, the braincase is poorly defined, in part due to vivianite buildup but perhaps also to the susceptibility of thin-walled sinuses to dissolution under conditions of low tissue pH. The intracranial space in Khroma is better defined and was segmented as a unit separate from the cranium. In mammals, the endocranial surface conforms generally to the shape of the brain, so this "virtual endocast" provides a reasonable portrait of a neonate mammoth's brain. Linear measurements of the endocast are given (caption of Fig. 11), and its volume is approximately  $2,300 \text{ cm}^3$ .

**Skull shape.**—Lyuba's skull is conspicuously narrower than Khroma's (Fig. 12). Part of this is clearly a result of postmortem deformation, seen also in the approximation of mandibular rami evident in anterior view (Fig. 12.1), which may have been facilitated by dissolution of bone due to lactic acid accumulation within Lyuba's tissues. The clearest example of shape difference not due to postmortem events is that in dorsal view, Lyuba's premaxillae are narrower (minimum width, 58 mm) than Khroma's (minimum width, 82 mm) and have their narrowest point located more posteriorly (Fig. 12.2). There is also a thickened extension of the alveolar margin of the premaxillae in

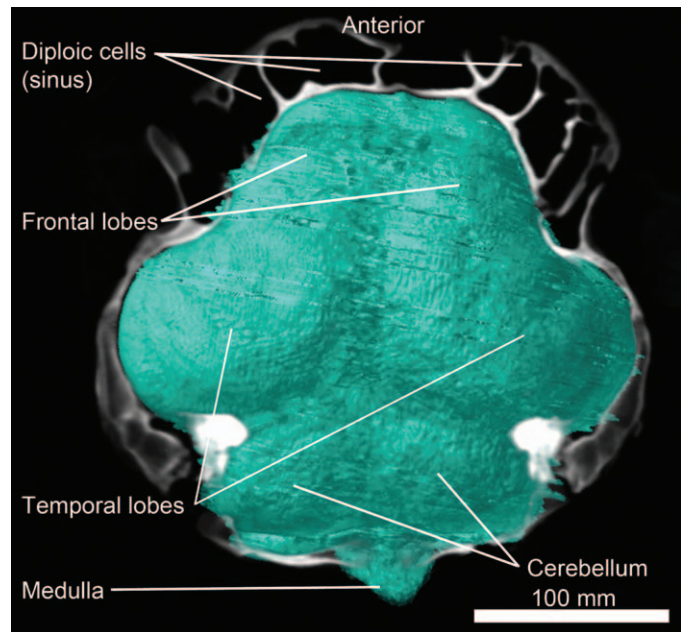


FIGURE 11—Khroma's endocranial space, segmented from the Le Puy scan and represented as a 3-D volume in an oblique, approximately dorsal aspect. This is shown in conjunction with a slice-view of surrounding cranial bone, intersecting the forehead just above the orbits, and tilted ventrally toward the posterior, to intersect the petrosals (well-ossified bones [bright white] within the basicranial complex). Maximum transverse width of endocast is 225 mm, maximum dorsoventral depth is 118 mm, and maximum anteroposterior length is 205 mm.

Khroma that is absent in Lyuba. This structure surrounds the milk tusk sockets and is also present in muscle, fat and dermal layers.

An unusual, but discretely developed radiodensity anomaly occurs within the dermal layer of tissue on Lyuba's skull, just left of the midline and dorsal to her external nares (visible in Fig.

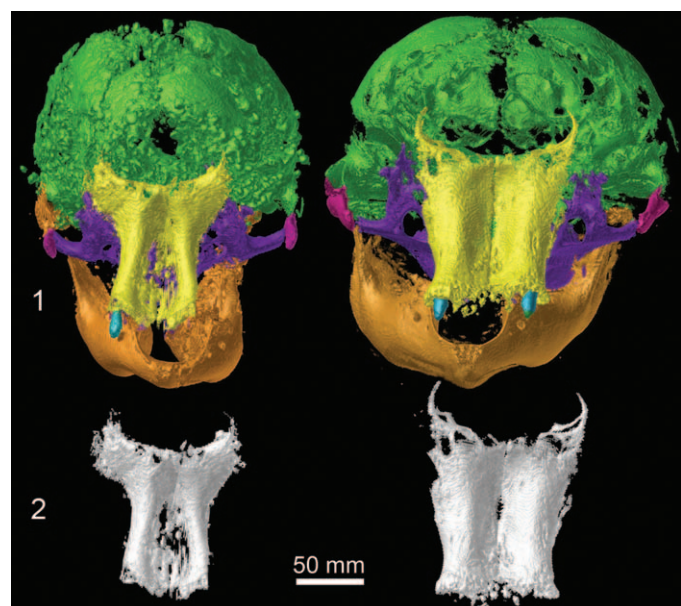


FIGURE 12—Crana and mandibles of Lyuba and Khroma compared: 1, Lyuba's skull (on left) is narrower than that of Khroma (on right); 2, in anterodorsal aspect, Lyuba's premaxillae (on left) are narrower and less robust than Khroma's (on right). Scale applies to all images. Color scheme as in Figure 1 (but nasals included with frontal/parietal complex). Milk tusks (right only for Lyuba) shown as turquoise.

12.1, left, and mentioned in the caption for Fig. 3). This structure is conical and much more symmetrical than the “typical” vivianite nodules that surround it. We propose that this could be a partially calcified hematoma, implying localized impact, possibly even associated with birth (ca. one month prior to death). Such an injury does not seem severe enough to give rise to developmental abnormalities.

**Teeth.**—Milk tusks and deciduous premolars (upper and lower for Lyuba, lowers only for Khroma) were removed from one side of each animal. Our histologic and compositional analyses of these specimens are published (Rountrey et al., 2012), were discussed above (Khroma’s age at death), or will be presented elsewhere. Our focus here is on use of microCT as a means of documenting dental morphology. Before any destructive analysis, each specimen’s 3-D form was recorded. For milk tusks and Lyuba’s anteriormost cheek teeth ( $dP^2$  and  $dP_2$ ), which were relatively simple in shape and were extracted with no adherent tissue, silicone molding methods were adequate. Lyuba’s next cheek teeth ( $dP^3$  and  $dP_3$ ), like most mammoth cheek teeth at such an early stage of development, presented an intricate system of closely juxtaposed surfaces and confined spaces. This complex morphology makes traditional molding and casting essentially impossible. Khroma’s deciduous premolars further complicated matters in that they were extracted with adherent soft tissue.

In addition to capturing the external form of teeth, we were interested to have a 3-D record that distinguished enamel and dentin, and microCT accomplished this readily. For the most part, cementum had not begun to form on these teeth, which is why their crowns present such an open, apparently unsupported structure. The digital models that resulted from microCT provide a level of detail far beyond what could be accomplished in any other way (Fig. 13.1). They also provided the basis for physical models that were more than adequate, if coarser than their digital counterparts. Some parts of roots and developing lamellae were so delicate that a physical copy would be too fragile to survive production and handling. Tooth parts that were thinner than approximately one millimeter were digitally thickened, and the resulting file (Fig. 13.2, 13.3) was used to generate rapid prototypes that capture most morphologic features of the teeth (Fig. 13.4, 13.5).

#### DISCUSSION AND CONCLUSIONS

CT data reveal a great deal about the morphology, circumstances of death, and diagenetic history of these two specimens. Both Lyuba and Khroma died from aspirating sediment, Lyuba in a lacustrine setting, and Khroma in some setting that also resulted in a mid-thoracic fracture. Khroma, for example, could have been a victim of a mud flow or an instance of bank collapse that produced this trauma. After death, Lyuba was apparently subjected to microbiologically mediated alteration that produced authigenic vivianite within her tissues in loci controlled by concentrations of iron that reflect her physiological state in the last moments of her life (Fisher et al., 2012). Lyuba’s body was also affected by forces that produced lateral (in an anatomical reference frame) compression and some shear. One of the open issues about this concerns how she was oriented in burial. If she was recumbent, on one side, the compression could have been a consequence of sediment compaction. If she was buried in a more upright position, lateral forces would be implicated, which could have resulted from development of ice wedges. The secondary context from which she was recovered makes this difficult to resolve.

Segmentation based on CT data provides subtle and comprehensive detail, not only on perimortem and diagenetic events, but also on fundamental aspects of osteology (online Supplemental Data file 1). Lyuba and Khroma’s skeletons are

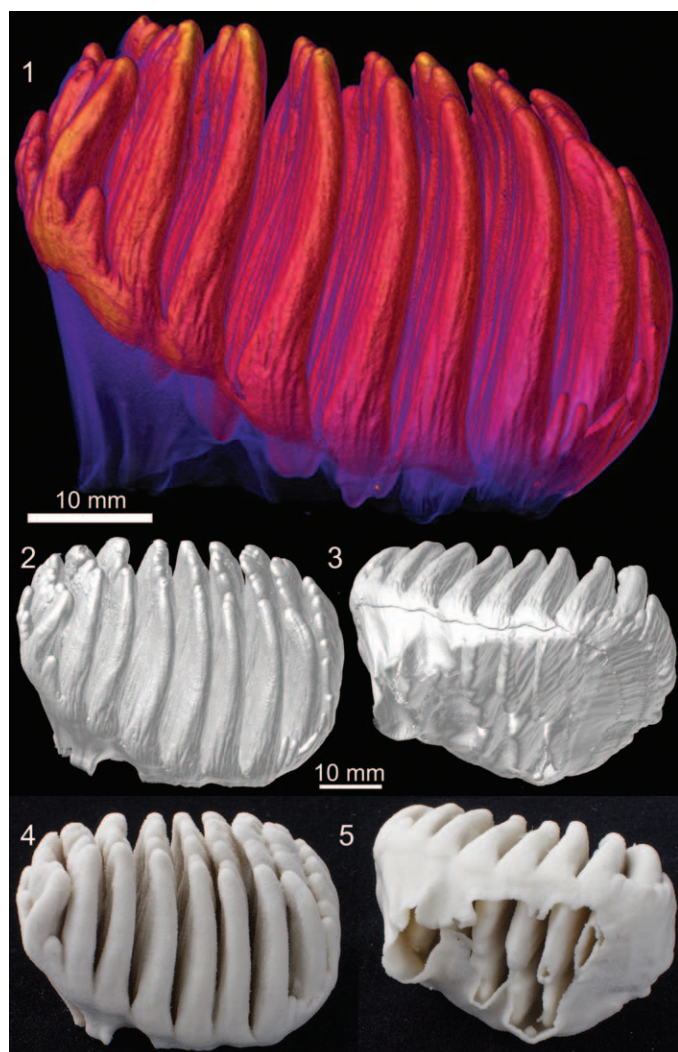


FIGURE 13—Lyuba’s left  $dP^3$ : 1, digital model in lingual aspect (radiodensity is scaled from red/more dense/enamel to blue/less dense/dentin); 2, digital surface model in oblique lingual-occlusal view; 3, digital surface model looking into pulp cavity; 4, rapid prototype, oriented as in 2; 5, rapid prototype, oriented as in 3. Common scale for 2–5.

similar in both morphology and stage of development. Some of the differences we observe could represent individual or population-level variation. While climate and habitat may have been similar for these two animals, the populations to which they belonged were separated by nearly 5,000 km. In addition, these mammoths clearly differed in geologic age, even if to an extent that is not well constrained. Finally, many differences between them, including their intriguingly disparate premaxillae, could reflect ontogenetic change. One additional month of growth, in Khroma as compared to Lyuba, may seem like a minor factor, but if young mammoths grew and ossified their skeletons rapidly, it may have had a marked effect.

Comparisons to published data on other specimens are interesting but bring up the same issues regarding possible sources of variation. For example, Maschenko (2002) has done a great deal to assemble a framework for determining age and developmental stage in mammoths, and age-controlled comparisons with Lyuba and Khroma (e.g., Maschenko, 2002, tables 13–16 for humeri, ulnae, femora, and tibiae, respectively) indicate that many of his specimens are smaller than Lyuba and Khroma. However, some of these same specimens come from

the Sevsk locality, where even adults are remarkably small in body size, so this may be a population-level difference. Regardless of the specifics for single localities, anatomically comprehensive data on single individuals such as Lyuba and Khroma, will serve as standards for future syntheses in our understanding of mammoth skeletal and dental development.

Our segmentation of Khroma's endocranial space represents a first step in the comparison of brain development in mammoths and other proboscideans, with potential implications for life history and behavioral traits that may be associated. Brain size in modern elephant neonates is 2,500 cm<sup>3</sup> (Shoshani et al., 2006). Data currently available from modern elephants are limited to volume estimates based on mass, and such estimates depend critically on tissue condition at the time of analysis. Nonetheless, the difference between mammoths and elephants tends to support the idea of a slightly shorter gestation period in mammoths, proposed also by Maschenko (2002).

These and other hints concerning the life histories of mammoths and how they changed, approaching the time of extinction, offer our best chance for understanding the cause of that extinction.

#### ACKNOWLEDGMENTS

We thank S. Smith and I. Rahman for inviting us to participate in the symposium "Virtual Paleontology: computer-aided analysis of fossil form and function." We also appreciate help from S. Gorbunov and L. Hannell of the International Mammoth Committee, S. Grishin and G. Karzanova of the Shemanovskiy Museum and Exhibition Center, G. Savvinov and S. Fedorov of the Institute of Applied Ecology of the North, M. Jones and staff at the Nondestructive Evaluation Laboratory of Ford Motor Company, Livonia, Michigan, M. Lynch of the University of Michigan School of Dentistry µCT Core (funded in part by NIH/NCRR S10RR026475-01), and staff of GE Healthcare in Waukesha, Wisconsin (USA), Centre Hospitalier Universitaire in Clermont-Ferrand (France), and Centre Hospitalier Emile Roux in Le Puy-en-Velay (France). We are grateful for financial support from U.S. National Science Foundation grant EAR-0545095 to DCF and National Geographic grants EC-03494-08 and CRE-8503-08 to DCF and to the editors and two reviewers for comments that improved the manuscript.

#### ACCESSIBILITY OF SUPPLEMENTAL DATA

Supplemental data deposited in Dryad repository: <http://dx.doi.org/10.5061/dryad.d03qr>.

#### REFERENCES

- BARNES, I., B. SHAPIRO, A. LISTER, T. KUZNETSOVA, A. SHER, D. GUTHRIE, AND M. G. THOMAS. 2007. Genetic structure and extinction of the woolly mammoth, *Mammuthus primigenius*. *Current Biology*, 17:1,072–1,075.
- BLUMENBACH, J. F. 1799. *Handbuch der Naturgeschichte* (sixth edition). Dieterich, Göttingen.
- BOESKOROV, G., A. N. TIKHONOV, AND P. A. LAZAREV. 2007. A new find of a mammoth calf. *Doklady Biological Sciences*, 417:480–483.
- DEBRUYNE, R., G. CHU, C. E. KING, K. BOS, M. KUCH, C. SCHWARZ, P. SZPAK, D. R. GRÖCKE, P. MATHEUS, G. ZAZULA, D. GUTHRIE, D. FROESE, B. BUIGUES, C. DE MARLIAVE, C. FLEMMING, D. POINAR, D. FISHER, J. SOUTHON, A. N. TIKHONOV, R. D. E. MACPHEE, AND H. N. POINAR. 2008. Out of America: ancient DNA evidence for a New World origin of late Quaternary woolly mammoths. *Current Biology*, 18:1–7.
- ENK, J., A. DEVault, R. DEBRUYNE, C. E. KING, T. TREANGEN, D. O'ROURKE, S. L. SALZBERG, D. FISHER, R. MACPHEE, AND H. POINAR. 2011. Complete Columbian mammoth mitogenome suggests interbreeding with woolly mammoths. *Genome Biology* 2011, 12:R51.
- FALCONER, H. 1857. On the species of mastodon and elephant occurring in the fossil state in Great Britain. Part 1. *Mastodon*. *Quarterly Journal of the Geological Society of London*, 13:307–360.
- FISHER, D. C. 1996. Extinction of proboscideans in North America, p. 296–315. In J. Shoshani and P. Tassy (eds.), *The Proboscidea: Evolution and Palaeoecology of Elephants and their Relatives*. Oxford University Press, Oxford.
- FISHER, D. C. 2009. Paleobiology and extinction of proboscideans in the Great Lakes region of North America, p. 55–75. In G. Haynes (ed.), *American Megafaunal Extinctions at the End of the Pleistocene*. Springer Science + Business Media, New York.
- FISHER, D. C., A. N. TIKHONOV, P. A. KOSINTSEV, A. N. ROUNTREY, B. BUIGUES, AND J. V. D. PLICHT. 2012. Anatomy, death, and preservation of a woolly mammoth (*Mammuthus primigenius*) calf, Yamal Peninsula, northwest Siberia. *Quaternary International*, 255:94–105.
- GOODEN, B. A. 1994. Mechanism of the human diving response. *Integrative Physiological and Behavioral Science*, 29:6–16.
- GUTHRIE, R. D. 1990. *Frozen Fauna of the Mammoth Steppe: The Story of Blue Babe*. University of Chicago Press, Chicago, Illinois, 323 p.
- HANLON, S., G. NAGEL, R. BOYD, R. LEWSHENIA, M. FORSBERG, AND S. GHEUNG. 1971. The dissociation of bovine hemoglobin at acid pH. *Biochimica et Biophysica Acta*, 229:359–367.
- HOUNSFIELD, G. N. 1980. Computed medical imaging (Nobel lecture, 8 December 1979). *Journal of Radiology*, 61:459–468.
- JOHANSEN, K. 1964. Regional distribution of circulating blood during submersion asphyxia in the duck. *Acta Physiologica Scandinavica*, 62(1–2):1–9.
- KOSINTSEV, P. A., E. G. LAPTEVA, S. S. TROFIMOVA, O. G. ZANINA, A. N. TIKHONOV, AND J. V. D. PLICHT. 2010. The intestinal contents of a baby woolly mammoth (*Mammuthus primigenius* Blumenbach, 1799) from the Yuribey River (Yamal Peninsula). *Doklady Akademii Nauk*, 432:556–558.
- KOSINTSEV, P. A., E. G. LAPTEVA, S. S. TROFIMOVA, O. G. ZANINA, A. N. TIKHONOV, AND J. V. D. PLICHT. 2012. Environmental reconstruction inferred from the intestinal contents of the Yamal baby mammoth Lyuba (*Mammuthus primigenius* Blumenbach, 1799). *Quaternary International*, 255:231–238.
- LAZAREV, P., S. GRIGORIEV, AND V. PLOTNIKOV. 2010. Mammoth calves from the permafrost of Yakutia. *Quaternaire, Hors-Série*, 3:56–57.
- LILLIE, R. D. 1939. Experiments on the solubility of hemosiderin in acids and other reagents during and after various fixations. *The American Journal of Pathology*, 15:225–239.
- LISTER, A. M. AND A. V. SHER. 2001. The origin and evolution of the woolly mammoth. *Science*, 294:1,094–1,097.
- LISTER, A. M., A. V. SHER, H. VAN ESSEN, AND G. WEI. 2005. The pattern and process of mammoth evolution in Eurasia. *Quaternary International*, 126–128:49–64.
- LISTER, A. AND P. BAHN. 2007. *Mammoths: Giants of the Ice Age* (revised edition). University of California Press, Berkeley, California, 192 p.
- MANNING, P. G., T. P. MURPHY, AND E. E. PREPAS. 1991. Intensive formation of vivianite in the bottom sediments of mesotrophic Narrow Lake, Alberta. *Canadian Mineralogist*, 29:77–85.
- MASCHENKO, E. 2002. Individual development, biology and evolution of the woolly mammoth. *Cranium*, 19:1–120.
- MASCHENKO, E., A. N. TIKHONOV, R. D. E. MACPHEE. 2005. Mammoth calf from Bolshoi Lyakhovskii Island (New Siberian Islands, Arctic Siberia). *Russian Journal of Thoriology*, 4:79–88.
- McGOWAN, G. AND J. PRANGNELL. 2006. The significance of vivianite in archaeological settings. *Geoarchaeology: An International Journal*, 21:93–111.
- METCALFE, J. Z., F. J. LONGSTAFFE, AND G. D. ZAZULA. 2010. Nursing, weaning, and tooth development in woolly mammoths from Old Crow, Yukon, Canada: implications for Pleistocene extinctions. *Palaeogeography, Palaeoclimatology, Palaeoecology*, 298:257–270.
- NESTI, F. 1825. Sulla nuova specie di elefante fossile del Valdarno all'Illustrissimo sig. Dott. Prof. Ottaviano Targioni Tozzetti. (Lettere sopra alcune ossa fossili del Valdarno non per anco descritte.) *Nuovo Giornale de' Letterati*, 11(24):195–216.
- PABST, M. AND F. HOFER. 1998. Deposits of different origin in the lungs of the 5,300-yr-old Tyrolean iceman. *American Journal of Physical Anthropology*, 107:1–12.
- PINEY, A. 1922. The anatomy of the bone marrow: with special reference to the distribution of the red marrow. *The British Medical Journal*, 2:792–795.
- POHLIG, H. 1885. Über ein Hipparionen-fauna von Maragha in Nord-Persien, über fossile Elefantenreste Kaukasiens und Persiens, und über die Resultate einer Monographie der fossilen Elefanten Deutschlands und Italiens. *Zeitschrift der Deutschen Geologischen Gesellschaft*, 37:1,022–1,027.
- RAMSAY, E. C. AND R. W. HENRY. 2001. Anatomy of the elephant foot, p. 9–12. In B. Csuti, E. L. Sargent, and U. S. Bechert (eds.), *The Elephant's Foot*. Iowa State University Press, Ames, Iowa.
- ROUTREY, A. N. 2009. Life histories of juvenile woolly mammoths: stable isotope and elemental analyses of tooth dentin. Unpublished Ph.D. dissertation, University of Michigan, 331 p.
- ROUTREY, A. N., D. C. FISHER, S. VARTANYAN, AND D. L. FOX. 2007. Carbon and nitrogen isotope analyses of a juvenile woolly mammoth tusk: evidence of weaning. *Quaternary International*, 169–170:166–173.

- ROUNTREY, A. N., D. C. FISHER, A. N. TIKHONOV, P. A. KOSINTSEV, P. A. LAZAREV, G. BOESKOROV, AND B. BUIGUES. 2012. Early tooth development, gestation, and season of birth in mammoths. *Quaternary International*, 255: 196–205.
- SACHER, G. A. AND E. F. STAFFELDT. 1974. Relation of gestation time to brain weight for placental mammals: implications for the theory of vertebrate growth. *The American Naturalist*, 108:593–615.
- SHOSHANI, J., W. J. KUPSKY, G. H. MARCHANT. 2006. Elephant brain Part I: gross morphology, functions, comparative anatomy, and evolution. *Brain Research Bulletin*, 70:124–157.
- TOLMACHOFF, I. P. 1929. The carcasses of the mammoth and rhinoceros found in the frozen ground of Siberia. *Transactions of the American Philosophical Society, New Series*, 23:i–x, 11–74b.
- VAN GEEL, B., D. C. FISHER, A. N. ROUNTREY, J. VAN ARKEL, J. F. DUIVENVOORDEN, A. M. NIEMAN, G. B. A. VAN REENEN, A. N. TIKHONOV, B. BUIGUES, AND B. GRAVENDEEL. 2011. Palaeo-environmental and dietary analysis of intestinal contents of a mammoth calf (Yamal Peninsula, northwest Siberia). *Quaternary Science Reviews*, 30:3,935–3,946.
- VARTANYAN, S., V. GARUTT, A. SHER. 1993. Holocene dwarf mammoths from Wrangel Island in the Siberian Arctic. *Nature*, 362:337–340.
- VARTANYAN, S., KH. ARSLANOV, J. KARHU, G. POSSNERT, L. SÜLERZHITSKY. 2008. Collection of radiocarbon dates on the mammoths (*Mammuthus primigenius*) and other genera of Wrangel Island, northeast Siberia, Russia. *Quaternary Research*, 70:51–59.
- WARWICK, R. AND P. L. WILLIAMS. 1973. *Gray's Anatomy* (35th British edition). W. B. Saunders Co., Philadelphia, Pennsylvania, 1471 p.
- WEISSENGRUBER, G. E., G. F. EGGER, J. R. HUTCHINSON, H. B. GROENEWALD, L. ELSSÄSSER, D. FAMINI, AND G. FORSTENPOINTNER. 2006. The structure of the cushions in the feet of African elephants. *Journal of Anatomy*, 209:781–792.

ACCEPTED 8 OCTOBER 2013